

Ocean Eddies and Atmospheric Noise Drive Mixed Layer Depth Variability in the Southern Ocean

Yu Gao¹, Igor Kamenkovich², Benjamin Kirtman^{2,3}

¹Scripps Institution of Oceanography, University of California, San Diego, 9500 Gilman Drive, La Jolla, CA, 92093, USA

²Rosenstiel School of Marine, Atmospheric and Earth Sciences, University of Miami, 4600 Rickenbacker Causeway, Miami, FL, 33149, USA

³Frost Institute for Data Science and Computing, University of Miami, 4600 Rickenbacker Causeway, Miami, FL, 33149, USA

Key Points:

- Simulations that account for ocean eddies show a significantly deeper average mixed layer depth (MLD) compared to those that do not account for eddy effects.
- In regions with strong eddy activities, reduced atmospheric noise in simulations results in higher MLD variability, driven more by increased ocean current variability than by reduced atmospheric influence.
- Atmospheric noise suppresses ocean's natural variability, particularly diminishing the ocean's inherent influence on MLD variations during ocean-atmosphere coupling.

Abstract

We investigate the impact of atmospheric noise and model resolution on the relationship between oceanic currents, SST, and mixed layer depth (MLD) in the Southern Ocean, using global climate simulations and interactive ensemble experiments with the NCAR Community Climate System Model version 4.0, at both low (LR) and high spatial resolution (HR) in the ocean. Atmospheric noise is the variability from internal atmospheric dynamics, independent of low-frequency changes or anomalies in boundary conditions or atmospheric composition. The interactive ensemble coupling approach reduces atmospheric noise at the air-sea interface, enabling us to isolate its impact by comparing interactive ensemble simulations to directly coupled (control) runs. We assess the importance of ocean mesoscale currents by contrasting LR and HR simulations. The HR simulations that resolves ocean eddies shows deeper MLD compared to the non-eddy-resolving simulations, which is most likely due to excessive re-stratification by the parameterized eddies in the non-eddy-resolving simulations. In the HR simulations, reduced atmospheric noise amplifies mesoscale ocean currents in the interactive ensemble, which leads to increased SST and MLD variance in the Antarctic Circumpolar Current and Western Boundary Current regions. Furthermore, wind stress feedback interacting with ocean eddies modulates Ekman transport in eddy-resolving simulations, whereas in non-eddy-resolving simulations, Ekman transport is solely driven by atmospheric noise. This study addresses a gap in understanding the importance of oceanic intrinsic variability in driving MLD variability and demonstrating that atmospheric noise suppresses ocean's natural variability during atmosphere-ocean coupling.

Plain Language Summary

This paper investigates how ocean currents and atmospheric noise affect the Southern Ocean's mixed layer depth (MLD) variability. The mixed layer is the ocean's upper layer where temperature and salinity are relatively constant. The study uses computer simulations to analyze the impact of ocean currents and atmospheric noise on MLD variability. The results show that ocean currents significantly impact MLD variability, and the atmospheric noise suppresses the intrinsic oceanic variability in driving the MLD variations during the atmosphere-ocean coupling. The study also highlights the importance of eddy-resolving simulations in capturing the impact of ocean mesoscale currents on MLD variability. The findings of this study can help us better understand the complex interactions between the ocean and atmosphere in the Southern Ocean and improve our ability to predict future changes in the ocean and climate.

1 Introduction

1.1 Ocean Mixed Layer Variability and Ocean Eddies

The ocean mixed layer plays a vital role in modulating exchanges of heat, freshwater, and gases such as oxygen and carbon dioxide between the atmosphere and the ocean. Consequently, changes in mixed layer depth (MLD) can have profound implications for climate modeling, affecting exchange rates between the atmosphere, upper ocean, and deep ocean. The entrainment of carbon-rich, oxygen-poor waters into the mixed layer drives the interannual variability of air-sea oxygen and carbon dioxide fluxes in the Southern Ocean (Verdy et al., 2007). Additionally, MLD can modulate air-sea interaction by changing the effective heat capacity of the upper ocean: a shallower MLD results in lower heat capacity and increased sensitivity of sea surface temperature (SST) to surface heat flux. At the same time, a deeper MLD leads to higher heat capacity and reduced SST sensitivity (Tozuka & Cronin, 2014). Therefore, the contribution of surface heat fluxes to surface frontogenesis and frontolysis depends on their gradients and the distribution of MLD (Tozuka et al., 2018; Gao et al., 2023).

The Southern Ocean is an integral part of the global overturning circulation since the upwelling in the Southern Ocean is a vital branch of the circulation (Speer et al., 2000; Marshall & Speer, 2012). The formation of the deep winter mixed layer has been linked to the intermediate water masses, Subantarctic Mode Water (SAMW) and Antarctic Intermediate Water (AAIW), in the Southern Ocean (McCartney, 1977; Rintoul, 2002; Sallée et al., 2006; J. Holte & Talley, 2009; Lee et al., 2011; J. W. Holte et al., 2012). These intermediate water masses control the ventilation of the thermocline of the subtropical gyres in the Southern Hemisphere and contribute to the changes in heat, carbon, and productivity globally (Sloyan & Rintoul, 2001; Sarmiento et al., 2004; Sallée et al., 2012). Therefore, it is essential that we understand the MLD variability in the Southern Ocean.

1.2 Atmospheric Noise and Interactive Ensembles

Atmospheric noise is defined here as the variability due to internal atmospheric dynamics independent of low-frequency variability or anomalies in boundary conditions (e.g., SST anomalies, soil moisture, snow cover, sea-ice) or in atmospheric composition (i.e., aerosols). For conceptual simplicity, the atmospheric forcing can be separated into signal and noise components: (1) SST-driven atmospheric variability, which is referred to as "signal", and (2) the stochastic internal dynamics that is not directly driven by Sea Surface Temperature Anomalies, which is referred to as "atmospheric noise".

SST-driven atmospheric variability (the "signal") refers to atmospheric response to mesoscale SST anomalies (Small et al., 2008). For example, Kirtman et al. (2012) demonstrates that the correlation between the upward turbulent heat fluxes and SST anomalies in the Southern Ocean is positive in simulations that resolve mesoscale eddies, which implies that the atmosphere dampens SST variability. As a result, ocean eddy amplitude is enhanced when mesoscale SST-driven atmospheric processes are absent in the air-sea coupling (Kirtman et al., 2017). Gao et al. (2022) shows that mesoscale currents induce SST anomalies that are subsequently dampened by atmospheric heat fluxes. SST anomalies also impact near-surface wind, cloud properties, and rainfall in the Southern Ocean by affecting turbulence in the atmospheric boundary layer (Frenger et al., 2013).

The role of the oceanic signal can be isolated using the interactive ensemble coupling strategy, which reduces the atmospheric noise at the air-sea interface. Barsugli & Battisti (1998) provides a stochastically forced conceptual model which shows the interaction between the atmosphere and ocean in midlatitudes amplifies variance within both systems and attenuates the energy exchange between them. The paper also mentions that a principal consequence of this air-sea thermal coupling is the mitigation of thermal damping in midlatitude regions. Additionally, the article states that this study serves as a foundational framework for future explorations using the interactive ensemble design. The interactive ensemble approach introduced an ensemble of atmospheric models coupled to one ocean model to isolate the impact of internal atmospheric variability (Kirtman & Shukla, 2002). Many previous studies have proven its utility for quantifying how mesoscale air-sea coupling affects climate predictability (Wu & Kirtman, 2005; Lopez & Kirtman, 2014; Kirtman et al., 2017; Bishop et al., 2017). For example, Kirtman et al. (2017) demonstrated that the ocean mesoscale activity increases model-estimated climate predictability by increasing the dependency of atmospheric internal dynamics on the SST-driven signal.

These studies suggest that neglecting mesoscale air-sea coupling can lead to inaccurate representation of ocean mesoscale variability, and potential biases in long-term climate modeling. This study will explore the importance of two main processes for mesoscale variability in MLD: 1) mesoscale oceanic currents, by comparing eddy-resolving to non-eddy-resolving ocean models; and 2) internal atmospheric noise at the air-sea interface, by using the interactive ensemble coupling technique.

Table 1. Global climate model configuration and experiments. Adapted from Kirtman et al. (2017)

Experiments	Ocean	Atmosphere	ensemble size
LRC	1°lat x 1°lon	0.5 °	1
LRIE	1 lat °x 1°lon	0.5 °	1 ocean, 10 atmosphere
HRC	0.1°lat x 0.1°lon	0.5 °	4
HRIE	0.1°lat x 0.1°lon	0.5 °	1 ocean, 10 atmosphere

2 Data and Methodology

2.1 Model Experiments and Data

The global climate simulations are based on the NCAR Community Climate System Model version 4.0 Gent et al. (2011). The atmospheric component is based on the Community Atmospheric Model version 4 and the oceanic part – the Parallel Ocean Program version 2 (Smith et al., 2010)). Kirtman & Shukla (2002) and Kirtman et al. (2017) describe the interactive ensemble coupling strategy and details of the experiments used in this study, so here we only provide brief descriptions. We analyze four experiments: two control experiments and two interactive ensembles, at both low- and high spatial resolution in the ocean (Table 1). The standard low-resolution (LRC experiment is a 255-year present-day climate simulation, where the first 40 years are considered spin-up. The LRC experiments use a 1° atmospheric model coupled to ocean and sea ice models with a zonal resolution of 1.2° and meridional resolution that varies from 0.27° at the equator to the 0.54° in the mid-latitudes. The high-resolution (HR) experiments are based on a 4-member ensemble where each ensemble also uses a present-day forcing. The HR experiments use a 0.5° atmospheric model coupled to 0.1° ocean and sea ice models. We analyze the monthly data between 35 °S to 60 °S to include most of the Southern Ocean while avoiding the region with sea ice. We also selected 30-year-long data from year 121 to 150 in each experiment for comparison. We plot an altimetry-derived geographical position of the Subantarctic Front (SAF) and Polar Front (PF) in each figure (Park & Durand, 2019).

2.2 Interactive Ensemble Technique

The intention of the interactive ensemble coupling strategy is to suppress the atmospheric noise at the sea surface. Multiple realizations (ensemble members) of the atmospheric component are coupled to a single realization of the ocean component. The ensemble-mean fluxes of heat, momentum, and freshwater from atmospheric ensemble members are used to force the ocean component, while each atmospheric ensemble member has the same SST forcing produced by the ocean component. This coupling technique is to have the ensemble mean of the atmospheric models continuously interact with the ocean model as the coupled system evolves (Kirtman & Shukla, 2002).

To estimate the coupling strength and identify processes that drive the SST variability, Kirtman et al. (2005), Kirtman et al. (2017) and Zhang & Kirtman (2019) applied SST variance ratio test based on the Hasselmann (1976) hypothesis. Here we provide a brief description of this conceptual model following their examples.

In the control experiment, in which one atmospheric model is coupled to one ocean model, we assume that an oceanic variable O (such as SST) and an atmospheric variable A at time "n+1" are determined by their values at the previous time:

$$A^{n+1} = \alpha O^n + \mu A^n + N \quad (1)$$

$$O^{n+1} = \beta A^n + \delta O^n + P \quad (2)$$

where μ and δ represent the memory of the previous state, and α and β are the coupling coefficients that are bounded between 0 and 1. N and P stand for the uncoupled internal noise in atmospheric and ocean components, respectively, which is assumed to be Gaussian and white. Ocean noise represents the effects of internal ocean dynamics, which include mesoscale advection.

In the interactive ensemble, multiple atmospheric models (ensemble members) are coupled to one ocean model. Assuming M is the number of atmospheric models that are coupled with one ocean model, the equations 1 can be generalized into a set of equations representing the atmospheric interactive ensembles:

$$A_1^{n+1} = \alpha O^n + \gamma A_1^n + N_1, \quad (3)$$

$$A_2^{n+1} = \alpha O^n + \gamma A_2^n + N_2, \quad (4)$$

$$\dots \quad (5)$$

$$A_M^{n+1} = \alpha O^n + \gamma A_M^n + N_M, \quad (6)$$

$$O^{n+1} = \frac{\beta}{M} \sum_{k=1}^M A_k^n + \delta O^n + P, \quad (7)$$

where the atmospheric models are represented by $A_1^n, A_2^n, \dots, A_M^n$ with internal noise N_1, N_2, \dots, N_M .

The ratio between variance in the control and IE simulations can serve to quantify the impact of atmospheric noise and interpret the interactive ensemble. Taking O in the above theoretical model to be SST, the variance ratio can be diagnosed in terms of the coupling strength and the amplitude of atmospheric and oceanic noise forcing:

$$\frac{\text{Variance}(SST_{IE})}{\text{Variance}(SST_{CTRL})} = \frac{\beta^2 \sigma_N^2 / M + \sigma_P^2}{\beta^2 \sigma_N^2 + \sigma_P^2} \quad (8)$$

where σ_N^2 and σ_P^2 is the variance of the internal atmospheric and oceanic noise, respectively. Following the example of Kirtman et al. (2017) and Zhang & Kirtman (2019), who applied the variance ratio test solely to SST, we broaden the application of their theoretical model to include additional oceanic variables, such as MLD and current speed. The variance ratio test applies to terms like MLD and currents since MLD is implicitly coupled to the atmosphere and currents are directly coupled via the wind stress. For example, we can quantify the impact of atmospheric noise and ocean noise on the MLD variability, by analyzing the ratio of the MLD variance in the IE to that in the control experiment:

$$\frac{\text{Variance}(MLD_{IE})}{\text{Variance}(MLD_{CTRL})} = \frac{\beta^2 \sigma_N^2 / M + \sigma_P^2}{\beta^2 \sigma_N^2 + \sigma_P^2} \quad (9)$$

where σ_N^2 and σ_P^2 is the variance of internal atmospheric and oceanic noise, respectively.

For LRIE and HRIE, there are $M = 10$ atmosphere components coupled to 1 ocean component (Table 1). Suppose the SST or MLD variance ratio is between 0.1 and 1.0. In that case, the ocean noise (internal ocean dynamics), coupled feedback, non-linearity,

or a combination of these three elements can play a role, and the variability is only partially forced by the atmospheric noise. If the SST or MLD variance ratio exceeds 1.0, the reduction of atmospheric noise in the interactive ensemble enhances the oceanic variance compared to the control experiment. We will conclude that, in this case, unstable coupling and non-linearity are essential, which means that a linear conceptual model cannot be used to explain the variability. In this case, the non-linear climate system can be chaotic in which the noise is "state-dependent", and the unstable coupled feedback affects the variability (Kirtman et al., 2017). Similarly, we can analyze the variance ratio of other oceanic variables, such as the surface current speed and Ekman transport.

3 Results

In this section, we first discuss the relationship between SST, MLD variability, and ocean currents by the eddy-resolving and non-eddy-resolving simulations. Hereafter, we use the terms "mesoscale ocean currents" and "ocean eddies" interchangeably, referring to ocean currents that occur at spatial scales of around 10 to 100 kilometers and temporal scales of days to months. We then explore the importance of atmospheric noise in SST and MLD variability by comparing the control simulations to the interactive ensemble.

3.1 Importance of ocean currents in SST variability

In high-resolution (HR) experiments, the variance of sea surface temperature (SST) is notably higher, particularly in Antarctic Circumpolar Current (ACC) regions and western boundary current regions, such as the Agulhas Current areas, when compared to the results of low-resolution (LR) experiments. There are several reasons why the HR experiments produce significantly higher and more realistic SST variability compared to the LR experiments: 1) heat advection by ocean eddies creates SSTA in regions with strong oceanic currents, which demonstrates that resolving Southern Ocean eddies is critical for getting the SST variability right; 2) MLD variability modulates the relationship between SSTA and the eddy advection of heat. The MLD in the HR experiment is deeper than in LRC and exhibits higher variance in general, which further enhances the importance of oceanic advection in SST variability. These effects improve the difference in SSTA variance between LR and HR experiments. Besides, these effects possibly increase the HRIE/HRC variance ratio by enhancing the importance of ocean dynamics compared to atmospheric noise.

3.2 Importance of ocean currents in MLD

We first discuss the relationship between MLD and SST. The climatological annual cycle has not been removed from these values, and the Variations are heavily influenced by seasonal variability. The variations of the MLD are negatively correlated with SST in most of the regions in the Southern Ocean (Fig.1 a-b), which means that cooler SST corresponds to deeper MLD. This is a relationship we can expect in seasonal variations in MLD, which deepens in winter and shoals in summer. However, this simple one-dimensional relationship breaks down in regions with strong oceanic currents, such as the Antarctic Circumpolar Current (ACC) and Western Boundary Currents (WBC, Fig.1 b). This breakdown is more pronounced in the HRC simulation than in LRC, largely because of fast time-mean oceanic currents (Fig.1) and stronger mesoscale variability (Fig.2 e-f) in HRC. The surface Eddy Kinetic Energy (EKE) is calculated as $EKE = 1/2(U'^2 + V'^2)$, where U' and V' are the velocity departure from the 30-year-mean surface current speed. Note that most of the variability in velocities comes from mesoscale currents, although the seasonal anomalies in current speed will also contribute to EKE.

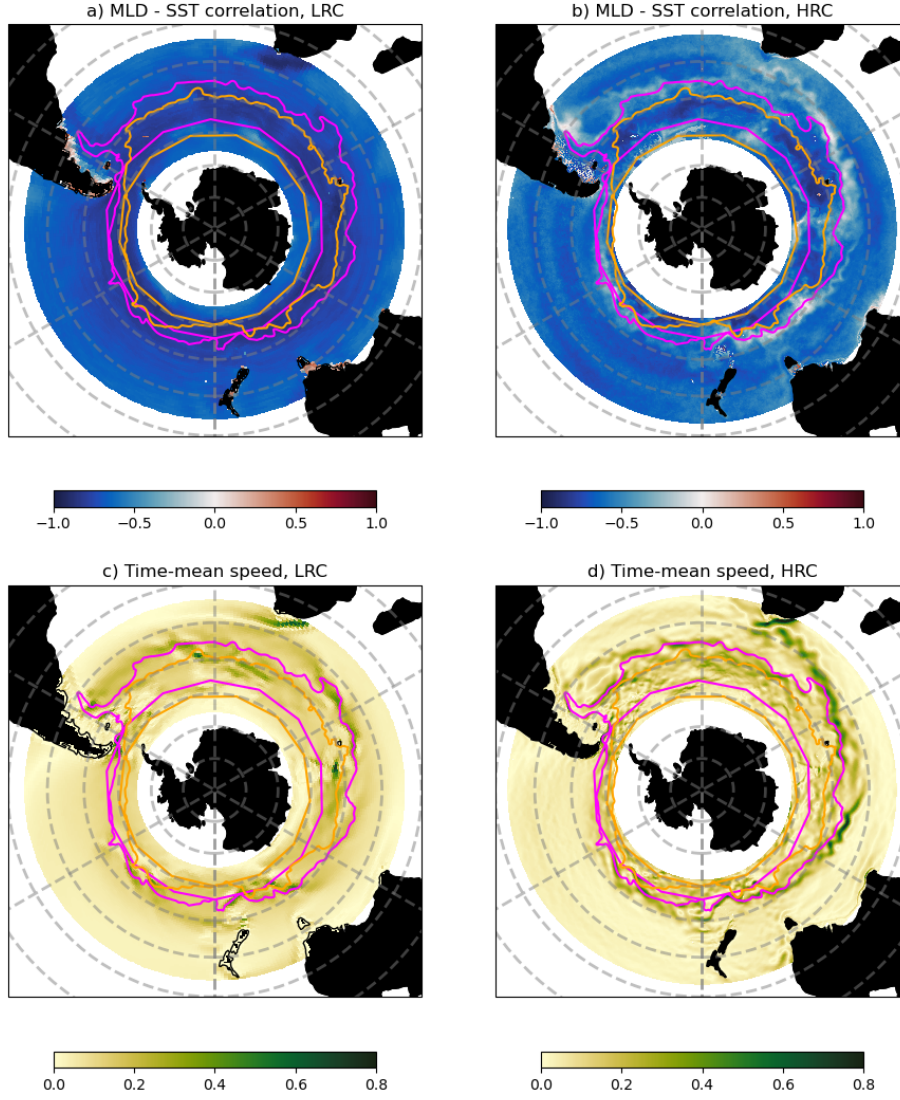


Figure 1. The correlation coefficient between the SST and MLD in a) LRC and b) HRC. The time-mean surface current speed in c) LRC and d) HRC, from year 121 to 150. Polar Front (PF, orange line) and Subantarctic Front (SAF, magenta line).

The weak relation between SST and MLD in the ACC region suggests that a one-dimensional atmospheric forced mixed layer model Kraus et al. (1967) does not apply in the regions of strong advection. This conclusion is in agreement with the findings of Gao et al. (2023) who concluded that the buoyancy advection shear by oceanic currents generally counteracts the atmospheric buoyancy forcing in driving the mixed layer variability.

The time-mean MLD in HRC is significantly deeper than that in LRC in most Southern (Fig. 2). This is consistent with Lee et al. (2011), who discovered that the winter MLD in eddy-permitting ocean simulations aligns closely with observed data, while the winter MLD in coarse-resolution ocean models tends to be too shallow. The most significant disparities were identified within the Agulhas Current system, where a higher

surface heat loss over the Agulhas Return Current and a deeper mixed layer were observed in eddy-permitting simulations. In this study, we also find significant differences between the HRC and LRC experiments in ACC and WBC regions, including the Agulhas Current system, part of the Brazil Current, and the Brazil–Malvinas Confluence (Fig.2a-b). In addition to the mean current strength, the difference between the HRC and LRC experiments is also dependent on EKE: the MLD in the HRC simulation is shallower in regions of higher EKE (WBC and ACC regions) and deeper in the other areas (Fig.2e-f).

It is unclear if we can explain the deepening of the MLD in HRC by the action of mesoscale eddies alone. On average, eddies are assumed to re-stratify the base of the mixed layer (Fox-Kemper et al., 2008; Fox-Kemper & Ferrari, 2008). At the same time, Gao et al. (2022) demonstrates that mesoscale buoyancy advection can also deepen the mixed layer, counteracting the atmospheric forcing. Additionally, mesoscale eddies are parameterized with the Gent & McWilliams (1990) scheme (hereafter "GM") in the non-eddy-resolving LRC and LRIE experiments and the model used by Lee et al. (2011). Therefore, it is possible that the GM parameterization overestimates the re-stratifying effects of mesoscale buoyancy advection. It is also worth noting that, in most of the Southern Ocean, the SST in HRC is significantly warmer than that in LRC Kirtman et al. (2012) and cannot explain the deeper MLD in HRC. Therefore, it is sensible to assume the importance of ocean buoyancy advection in driving the MLD variability.

The reduction of atmospheric noise in LRIE relative to LRC mostly leads to deepening of MLD north of the SAF and to shoaling of MLD south of the SAF (Fig.2a). Therefore, the southerly slope of MLD is generally reduced due to atmospheric noise. The time-mean MLD in LRIE is, in contrast, shallower than in the HRC experiment in most regions of the Southern Ocean, except the Agulhas Current region, part of the Brazil Current, and the Brazil–Malvinas Confluence region (Fig.2b). Gao et al. (2023) concludes that the atmospheric forcing and mixing induce MLD variability, while the oceanic advection of buoyancy essentially balances these atmospheric effects. With the reduction of atmospheric forcing, the strong buoyancy advection in ACC and WBC regions can become unbalanced and lead to the deepening of MLD.

3.3 Importance of atmospheric noise in SST variability

The response of SST variability to the reduction in the atmospheric noise in the interactive ensemble simulations differs between HR and LR simulations. Here SST anomalies (SSTAs) are defined as the departure from the monthly climatology. The absence of eddies in LRC leads to the lower SSTA variance (Fig.4) than in HRC, which is not surprising given weaker buoyancy advection in the LR case. Consistent with this result, the variance ratio (Fig.3) is also lower than in the HR simulations, which suggests that SSTAs are primarily caused by the anomalies in the atmospheric forcing, which are significantly reduced in LRIE. The following analysis suggests that the importance of atmospheric noise is overestimated in the LR simulations.

The noise reduction in LRIE relative to HRC enhances the SST variability in the ACC and WBC regions, where SSTA variance ratio exceeds 1.0 (Fig.3). This result is consistent with the findings in Kirtman et al. (2017). The results suggest that the SST variability in these regions is attributed to the intrinsic ocean dynamics, unstable coupled feedback and nonlinear dynamics. This is consistent with Gao et al. (2022) who found that the SSTA variability in the Southern Ocean in the regions with fast oceanic currents is driven by the intrinsic ocean dynamics rather than the atmospheric forcing. In other regions, the variance ratio is mostly between 0.5 and 1.0, which suggests the SSTA variability is partially driven by atmospheric noise and partially by coupled feedback, ocean eddies or non-linearity, or a combination of the three. In addition, the SSTA variance ratio can exceed 2.0 in the regions south of 60S, and these values may be exaggerated.

ated by biases in the Antarctic sea ice and excessive westerly winds in CCSM4 (Kirtman et al., 2017). The enhanced SST variance in the interactive ensemble simulations is consistent with the increase in the upper-ocean currents, which is discussed in the next section.

3.4 Importance of atmospheric noise in MLD variability

The air-sea interaction over Southern Ocean eddies can produce substantial MLD variability, which is underestimated in the non-eddy-resolving ocean models (Fig.5). MLD anomalies (MLDAs) are defined as the departure from the monthly climatology. Gao et al. (2023) suggests that oceanic mesoscale currents compensate the atmosphere-induced variations in MLD: while the atmospheric forcing and oceanic vertical mixing induce the MLD variability, the oceanic advection of buoyancy counteracts these atmospheric effects. The anomalies in atmospheric fluxes result either from intrinsic atmospheric variability or from an SST-forced response. The analysis of this section will help to estimate the relative importance of these two processes because the IE reduces the former, internal source for variability.

In both the HRIE and LRIE experiments, the MLDA variance is suppressed in most regions because of the reduced atmospheric noise (Fig.6). The changes are nevertheless dramatically different between the LR and HR simulations. In the LR experiments, the MLDA variance ratio is below 0.5 in most of the Southern Ocean (Fig.6a), which suggests that MLDA variability is partially forced by the atmosphere noise, and partially results from the coupled feedback, non-linearity and ocean noise. In contrast, in the HR experiments, the MLDA variance ratio is not only overall higher, but exceeds 1.0 in the ACC and WBC regions (Fig.6b).

In the ACC and WBC regions, the MLDA variance in HRIE is enhanced due to the reduced atmospheric noise. The SSTA variance is also enhanced there (Fig.3), however, the correlation between the SST and MLD anomalies is low in these regions (Fig.1), which means that the increased SST variance cannot explain the increase in MLD variance. We can, however, explain the increased MLDA variance with our findings in Gao et al. (2023). There, we concluded that while the atmospheric forcing and oceanic vertical mixing induce MLD variability, the oceanic advection of buoyancy counteracts these atmospheric effects. Results of Gao et al. (2023) further show that when mesoscale anomalies are removed from the surface fluxes of heat and momentum, the MLD variability can increase, and this effect is most pronounced in local winter. These conclusions suggest that when the atmospheric stochastic forcing is suppressed in HRIE, the oceanic advection can become partially unbalanced and enhance MLD variance.

More variance ratio test on the surface current speed. In the LR experiment (Fig.7a), the surface current variance ratio is mostly between 0.1 and 1.0, which suggests a combination of the atmospheric noise and internal dynamics drives surface present variability. In the HR experiments, in contrast, the current speed variance ratio is larger than 1.0 in most of the Southern Ocean (Fig.7b). This means the speed variance in HRIE increases due to the reduced atmospheric noise. The increase is especially pronounced in the Southern Indian and Atlantic sectors of the Southern Ocean, indicating the critical role of unstable coupling and nonlinearity. In contrast, the ratio is less than 1.0 in the Pacific sector (Fig.7). This pattern is similar to the MLDA variance ratio, which is also lower in the Pacific sector of the Southern Ocean (Fig.6). The similarity suggests the importance of ocean advection in MLD variance. The current speed and EKE are not as strong in the Southern Pacific sector (Fig.1 and Fig.2), and the ocean-atmosphere interactions have more considerable relative importance.

Compared to the SSTA variance ratio, HR experiments exhibit smaller regions where the MLDA variance ratio exceeds 1.0. This difference indicates that atmospheric noise plays a bigger role in driving MLD variability than SST variability. Atmospheric noise,

such as wind and air temperature variations, can significantly impact Mixed Layer Depth (MLD) more than Sea Surface Temperature (SST) due to the direct and immediate impact of wind stirring. This process mixes the ocean's surface layer to varying depths, leading to significant MLD variability. While SST is also affected by atmospheric conditions, the high heat capacity of the ocean means that a larger amount of heat exchange is required to alter its temperature significantly. Therefore, atmospheric noise tends to drive more variability in MLD than SST.

This heightened variability reflects a non-linear and unstable coupling. Essentially, this means that the relationship between the different forces (ocean currents, atmospheric noise, etc.) is not straightforward. Instead, these forces interact in complex, unpredictable ways, which is in nature of 'non-linearity.' 'Unstable coupling' indicates that the relationship between these elements isn't stable or consistent and can change rapidly.

This variability could be due to the increased Mixed Layer Depth (MLD), induced by the rise in atmospheric noise and atmosphere-driven mixing (Fig.6). As the MLD increases, the inertia (or resistance to change) in the upper ocean also increases. This could then lead to a decrease in ocean current variability. The state-dependence of atmospheric noise and the chaotic nature of the system could offer possible explanations for these observed phenomena.

This difference is, however, reversed in the LR simulations. The atmospheric noise mainly drives the SST variability in the LR experiments whereas the MLDA variance is due to a combination of the atmospheric noise, oceanic dynamics, and coupled feedbacks. Weaker oceanic currents and air-sea feedback onto SSTA in the LR simulations explain this.

3.5 Ocean Eddies Modulating Ekman Transport

To get further insight into the amplification of ocean currents in the absence of atmospheric noise, we investigate the response of Ekman transport to atmospheric forcing. The Ekman transport velocity (unit: m^2/s) in the u and v directions are calculated as below:

$$U_{Ekman} = \frac{\tau^y}{\rho_0 f}, \quad (10)$$

$$V_{Ekman} = \frac{-\tau^x}{\rho_0 f} \quad (11)$$

$$(12)$$

where τ^y and τ^x is the meridional and zonal wind stress at the sea surface, respectively. ρ_0 is the reference density (1025 kg/m^3) and f is the Coriolis parameter. We next calculate the variance in the magnitude of the Ekman transport $\sqrt{U_{Ekman}^2 + V_{Ekman}^2}$ and the variance ratio.

Fig.8 emphasizes the role of wind stress feedback and Southern Ocean eddies in shaping Ekman transport in our eddy-resolving experiments: the figure displays the influence of eddies on Ekman transport, as illustrated through the contrast between LR and HR experiments. Importantly, the figure shows a decrease in Ekman variance in response to reduced atmospheric noise, a trend that is more significant in HRIE than in LRIE. Fig.8 shows the impact of mesoscale currents on Ekman transport by comparing the LR and HR experiments. In LR experiment, the variance ratio is below 0.1, which indicates atmospheric noise alone drives the variability of the Ekman current speed. In HR experiment, the variance ratio is between 0.1 and 0.5, which suggests the Ekman transport variance is partially forced by the atmosphere noise, and partially by coupled feedback

and internal variability. For example, the presence of ocean eddies can modify Southern Ocean winds at the air-sea interface, which in turn alter the Ekman transport (Small et al., 2008; Frenger et al., 2013; Perlin et al., 2020). Mesoscale variability can also have an impact on wind stress through surface current speed correction: surface ocean currents modulate turbulent air-sea exchanges by changing the velocity shear between the atmosphere and oceanic surface. Current speed correction to the wind stress acts as a “top drag” (Dewar & Flierl, 1987; Duhaut & Straub, 2006; Gaube et al., 2015), since the enhanced Ekman pumping leads to relaxation of the thermocline. Importantly, the sensitivity of Ekman currents to atmospheric noise cannot explain amplification of surface currents in the HRIE simulations.

4 Summary and Discussion

The objective of this study is to explore the impact of atmospheric noise and model resolution on the relationship between oceanic currents, SST and MLD variability. This study utilizes the interactive ensemble coupling method, which reduces the atmospheric noise in both low- and high-resolution simulations. We analyzed the MLD variability and examined a variance ratio between the IE and control experiments, which allowed us to estimate the relative importance of the atmospheric noise in the MLD variability. Based on the analysis in Gao et al. (2022) and Gao et al. (2023), we expect variance based on monthly means to be a good measure of mesoscale anomalies. The impact of the strong oceanic currents, fronts and eddies were further assessed by comparing the eddy-resolving (HR) experiments to non-eddy-resolving (LR) experiments.

The strong negative correlation between SST and MLD breaks down in regions with strong large-scale currents and mesoscale activity, namely within the ACC fronts and in the WBC regions. The time-mean MLD is also significantly deeper in the presence of eddies even though SST in HR is warmer than in LR (Kirtman et al., 2012). Similarly, Lee et al. (2011) found the winter MLD in coarse-resolution coupled ocean model is too shallow. The MLD difference also depends on EKE: the MLD in HR simulations is shallower in regions of higher EKE and deeper elsewhere. These results suggest a crucial role of mesoscale ocean currents in driving SST and MLD anomalies. Eddies are widely assumed to re-stratify the ocean, but our results indicate that the GM parameterization may overestimate the re-stratifying role of ocean eddies. Gao et al. (2023) further demonstrates that the effects of eddies on MLD are more complex, and the corresponding buoyancy advection can even de-stratify the ocean below the mixed layer and deepen the MLD.

The results further demonstrate that SST variability is mainly driven by oceanic processes rather than atmospheric noise in the ACC and WBC regions. This result is consistent with Gao et al. (2022): the SST variability is driven by intrinsic ocean dynamics instead of atmospheric forcing. In such “quiet” regions of the Southern Ocean as the Pacific sector, the role of the atmosphere is more significant, and the SST variability is jointly driven by atmospheric noise and oceanic internal dynamics. Significantly, the reduction of the atmospheric noise in HRIE even enhances the SST variability in the ACC and WBC regions. However, it is still unclear why the SST variability is enhanced in these regions, and this topic deserves further investigation.

The atmospheric noise and the Southern Ocean eddies both control MLD variability. The differences between MLD variance ratio in LR and HR experiments demonstrate the importance of intrinsic ocean dynamics, especially in the ACC and WBC regions. Compared to the SST variability, however, the atmospheric forcing plays a more significant role in driving MLD variability in the HR experiments than in the LR runs. This result is consistent with Gao et al. (2023): in the Southern Ocean, SST variability is mainly driven by the intrinsic oceanic dynamic, while the MLD variability is caused by both atmospheric forcing and oceanic dynamics. Consistent with previous studies such as Zhang & Kirtman (2019), the atmospheric noise suppresses the upper-oceanic variability, and

the upper-ocean mesoscale variability in MLD, SST, and surface currents intensify in HRIE. Given a weak correlation between SST and MLD anomalies in these regions, it is natural to assume that the increase in SST and MLD variance in the absence of atmospheric noise are both caused by stronger oceanic currents. Gao et al. (2023) concludes that while the atmospheric forcing and oceanic vertical mixing induce MLD variability, the oceanic advection of buoyancy counteracts these atmospheric effects. Consistent with this finding, when the atmospheric stochastic forcing is suppressed in HRIE, the oceanic advection becomes unbalanced and can thus act to enhance MLD variance. Schneider et al. (2023) points out that ocean dynamics plays a minimal role in SO decadal variability in non-eddy-resolving models, which supports our conclusion that ocean mesoscale dynamics have a large role in SO variability. It is still, however, unclear why the variance in oceanic currents increase in HRIE, and this question deserves further investigation.

The suppression of surface currents by atmospheric noise cannot be explained by changes in the Ekman currents alone. The variance in the Ekman transport is decreased in HRIE and LR simulations, but the reduction is different between the LR and HR simulations for several reasons. The Ekman transport is modulated by the wind stress feedback over ocean eddies (SST anomalies) in the HR experiments, while the Ekman transport is driven solely by atmospheric noise in the LR experiments. Wind speed affected by SST anomalies, which created wind stress feedback to the ocean (Seo et al. (2016)). In the eddy-resolving experiments, the presence of ocean eddies can modify winds at the air-sea interface, which in turn alters the Ekman transport in the Southern Ocean (Small et al., 2008; Frenger et al., 2013; Perlin et al., 2020). The eddies also have an impact on the wind stress through surface current speed correction (Dewar & Flierl, 1987; O’Neill et al., 2003; Duhaut & Straub, 2006; Gaube et al., 2015). In other words, ocean eddies affect Ekman transport by modifying the wind forcing over the sea surface. Neglecting the eddy-wind coupling in non-eddy-resolving experiments may lead to imbalance in the zonal-mean steady-state circulation, since eddy-induced circulation compensates for the Ekman transport in the eddy-resolving models in the Southern Ocean (Abernathey et al., 2011; Marshall & Speer, 2012).

By examining the eddy-resolving and non-eddy-resolving experiments, we found that the air-sea interaction at mesoscale can cause significant differences in the variability of SST, MLD ocean currents, and Ekman transport. By comparing the interactive ensemble and control experiments, we conclude that non-eddy-resolving ocean models oftentimes overestimate the role of atmospheric noise and overlook the importance of ocean dynamics. In eddy-resolving ocean models, the ocean eddies, air-sea coupled feedback and non-linearity become more important to the mixed layer dynamics. We can further assess the eddy-induced effects on atmosphere-ocean coupling by using experiments with multiple ocean ensemble members coupled to one atmospheric component. Although running 10s global ocean models simultaneously is an ambitious task, we believe this is possible in the near future considering the fast development of computational power nowadays.

5 Open Research

The numerical model and data are available upon request. The Python code and jupyter notebook used to produce the results of this study are shared through the GitHub repository at https://github.com/yugaophd/SO_CCSM4.

Acknowledgments

This study is supported by the National Science Foundation (NSF) Research, USA, Award No. 1559151 and 1849990 and the National Aeronautics and Space Administration (NASA) grant No. 80NSSC20K1136. We would also like to acknowledge the following grants: National Oceanic and Atmospheric Administration (NOAA) grant NA18OAR4310293, NA15OAR4320064,

NA20OAR4320472, and NSF grant No. OCE1419569, OCE1559151 and AGS2241538. Benjamin P. Kirman is the William R. Middelthorn Chair of Earth Sciences and is grateful for the associated support. We acknowledge the computing resources provided by the University of Miami's Center of Computational Science and the high-performance computing support from Cheyenne provided by NCAR's Computational and Information Systems Laboratory, sponsored by NSF. We thank Dr. Michael Spall of Woods Hole Oceanographic Institution and Dr. Lisa Beal of the University of Miami for their helpful comments and suggestions. We also thank the editors and reviewers for their thoughtful comments.

References

- Abernathy, R., Marshall, J., & Ferreira, D. (2011). The dependence of southern ocean meridional overturning on wind stress. *Journal of Physical Oceanography*, 41(12), 2261 - 2278. Retrieved from <https://journals.ametsoc.org/view/journals/phoc/41/12/jpo-d-11-023.1.xml> doi: 10.1175/JPO-D-11-023.1
- Barsugli, J. J., & Battisti, D. S. (1998, February). The Basic Effects of Atmosphere–Ocean Thermal Coupling on Midlatitude Variability. *Journal of the Atmospheric Sciences*, 55(4), 477–493. Retrieved 2021-10-18, from [http://journals.ametsoc.org/doi/10.1175/1520-0469\(1998\)055<0477:TBEAO>2.0.CO;2](http://journals.ametsoc.org/doi/10.1175/1520-0469(1998)055<0477:TBEAO>2.0.CO;2) doi: 10.1175/1520-0469(1998)055<0477:TBEAO>2.0.CO;2
- Bishop, S. P., Small, R. J., Bryan, F. O., & Tomas, R. A. (2017, October). Scale Dependence of Midlatitude Air–Sea Interaction. *Journal of Climate*, 30(20), 8207–8221. Retrieved 2020-06-19, from <https://journals.ametsoc.org/jcli/article/30/20/8207/33173/Scale-Dependence-of-Midlatitude-AirSea-Interaction> doi: 10.1175/JCLI-D-17-0159.1
- Dewar, W. K., & Flierl, G. R. (1987). Some effects of the wind on rings. *Journal of Physical Oceanography*, 17(10), 1653 - 1667. Retrieved from https://journals.ametsoc.org/view/journals/phoc/17/10/1520-0485_1987_017_1653_seotwo_2_0_co_2.xml doi: 10.1175/1520-0485(1987)017<1653:SEOTWO>2.0.CO;2
- Duhaut, T. H. A., & Straub, D. N. (2006). Wind stress dependence on ocean surface velocity: Implications for mechanical energy input to ocean circulation. *Journal of Physical Oceanography*, 36(2), 202 - 211. Retrieved from <https://journals.ametsoc.org/view/journals/phoc/36/2/jpo2842.1.xml> doi: 10.1175/JPO2842.1
- Fox-Kemper, B., & Ferrari, R. (2008). Parameterization of mixed layer eddies. part ii: Prognosis and impact. *Journal of Physical Oceanography*, 38(6), 1166 - 1179. Retrieved from <https://journals.ametsoc.org/view/journals/phoc/38/6/2007jpo3788.1.xml> doi: 10.1175/2007JPO3788.1
- Fox-Kemper, B., Ferrari, R., & Hallberg, R. (2008). Parameterization of mixed layer eddies. part i: Theory and diagnosis. *Journal of Physical Oceanography*, 38(6), 1145 - 1165. Retrieved from <https://journals.ametsoc.org/view/journals/phoc/38/6/2007jpo3792.1.xml> doi: 10.1175/2007JPO3792.1
- Frenger, I., Gruber, N., Knutti, R., & Münnich, M. (2013, August). Imprint of Southern Ocean eddies on winds, clouds and rainfall. *Nature Geoscience*, 6(8), 608–612. Retrieved 2021-10-31, from <http://www.nature.com/articles/ngeo1863> doi: 10.1038/ngeo1863
- Gao, Y., Kamenkovich, I., & Perlin, N. (2023). Origins of mesoscale mixed-layer depth variability in the southern ocean. *Ocean Science*, 19(3), 615–627. Retrieved from <https://os.copernicus.org/articles/19/615/2023/> doi: 10.5194/os-19-615-2023
- Gao, Y., Kamenkovich, I., Perlin, N., & Kirtman, B. (2022). Oceanic advection controls mesoscale mixed layer heat budget and air–sea heat exchange in the southern ocean. *Journal of Physical Oceanography*, 52(4), 537 - 555. Re-

- trieved from <https://journals.ametsoc.org/view/journals/phoc/52/4/JPO-D-21-0063.1.xml> doi: <https://doi.org/10.1175/JPO-D-21-0063.1>
- Gaube, P., Chelton, D. B., Samelson, R. M., Schlax, M. G., & O'Neill, L. W. (2015). Satellite observations of mesoscale eddy-induced Ekman pumping. *Journal of Physical Oceanography*, 45(1), 104–132. Retrieved from <https://journals.ametsoc.org/view/journals/phoc/45/1/jpo-d-14-0032.1.xml> doi: 10.1175/JPO-D-14-0032.1
- Gent, P. R., Danabasoglu, G., Donner, L. J., Holland, M. M., Hunke, E. C., Jayne, S. R., ... Zhang, M. (2011, October). The Community Climate System Model Version 4. *Journal of Climate*, 24(19), 4973–4991. Retrieved 2021-02-26, from <https://journals.ametsoc.org/doi/10.1175/2011JCLI4083.1> doi: 10.1175/2011JCLI4083.1
- Gent, P. R., & McWilliams, J. C. (1990). Isopycnal mixing in ocean circulation models. *Journal of Physical Oceanography*, 20(1), 150–155. doi: 10.1175/1520-0485(1990)020<0150:IMIOCM>2.0.CO;2
- Hasselmann, K. (1976, December). Stochastic climate models Part I. Theory. *Tellus*, 28(6), 473–485. Retrieved 2021-10-21, from <http://tellusa.net/index.php/tellusa/article/view/11316> doi: 10.1111/j.2153-3490.1976.tb00696.x
- Holte, J., & Talley, L. (2009, September). A New Algorithm for Finding Mixed Layer Depths with Applications to Argo Data and Subantarctic Mode Water Formation. *Journal of Atmospheric and Oceanic Technology*, 26(9), 1920–1939. Retrieved 2021-10-08, from <http://journals.ametsoc.org/doi/10.1175/2009JTECH0543.1> doi: 10.1175/2009JTECH0543.1
- Holte, J. W., Talley, L. D., Chereskin, T. K., & Sloyan, B. M. (2012, March). The role of air-sea fluxes in Subantarctic Mode Water formation: SAMW Formation. *Journal of Geophysical Research: Oceans*, 117(C3), n/a–n/a. Retrieved 2020-06-18, from <http://doi.wiley.com/10.1029/2011JC007798> doi: 10.1029/2011JC007798
- Kirtman, B. P., Bitz, C., Bryan, F., Collins, W., Dennis, J., Hearn, N., ... Verstein, M. (2012, September). Impact of ocean model resolution on CCSM climate simulations. *Climate Dynamics*, 39(6), 1303–1328. Retrieved 2021-01-07, from <http://link.springer.com/10.1007/s00382-012-1500-3> doi: 10.1007/s00382-012-1500-3
- Kirtman, B. P., Pegion, K., & Kinter, S. M. (2005, July). Internal Atmospheric Dynamics and Tropical Indo-Pacific Climate Variability. *Journal of the Atmospheric Sciences*, 62(7), 2220–2233. Retrieved 2021-10-21, from <https://journals.ametsoc.org/doi/10.1175/JAS3449.1> doi: 10.1175/JAS3449.1
- Kirtman, B. P., Perlin, N., & Siqueira, L. (2017, December). Ocean eddies and climate predictability. *Chaos: An Interdisciplinary Journal of Nonlinear Science*, 27(12), 126902. Retrieved 2021-08-09, from <http://aip.scitation.org/doi/10.1063/1.4990034> doi: 10.1063/1.4990034
- Kirtman, B. P., & Shukla, J. (2002, May). Interactive coupled ensemble: A new coupling strategy for CGCMs: Interactive Coupled Ensemble. *Geophysical Research Letters*, 29(10), 5–1–5–4. Retrieved 2021-08-09, from <http://doi.wiley.com/10.1029/2002GL014834> doi: 10.1029/2002GL014834
- Kraus, E. B., Turner, J. S., & Hole, W. (1967). A one-dimensional model of the seasonal thermocline. *Tellus*, 9.
- Lee, M.-M., Nurser, A. J. G., Stevens, I., & Sallée, J.-B. (2011, August). Subduction over the Southern Indian Ocean in a High-Resolution Atmosphere–Ocean Coupled Model. *Journal of Climate*, 24(15), 3830–3849. Retrieved 2021-10-19, from <http://journals.ametsoc.org/doi/10.1175/2011JCLI3888.1> doi: 10.1175/2011JCLI3888.1
- Lopez, H., & Kirtman, B. P. (2014, September). WWBs, ENSO predictability, the apring barrier and extreme events: WWBs and ENSO Predictability.

- 592 *Journal of Geophysical Research: Atmospheres*, 119(17), 10,114–10,138. Re-
 593 trieved 2021-10-20, from <http://doi.wiley.com/10.1002/2014JD021908> doi:
 594 10.1002/2014JD021908
- 595 Marshall, J., & Speer, K. (2012, March). Closure of the meridional overturning
 596 circulation through Southern Ocean upwelling. *Nature Geoscience*, 5(3), 171–180.
 597 Retrieved 2021-11-02, from <http://www.nature.com/articles/ngeo1391> doi:
 598 10.1038/ngeo1391
- 599 McCartney, M. S. (1977). Subantarctic mode water. *A Voyage of Discovery, M. An-*
 600 *gel, Ed., Elsevier*, 103–119.
- 601 O'Neill, L. W., Chelton, D. B., & Esbensen, S. K. (2003). Observations of sst-
 602 induced perturbations of the wind stress field over the southern ocean on sea-
 603 sonal timescales. *Journal of Climate*, 16(14), 2340 - 2354. Retrieved from
 604 <https://journals.ametsoc.org/view/journals/clim/16/14/2780.1.xml>
 605 doi: 10.1175/2780.1
- 606 Park, Y.-H., & Durand, I. (2019, April). *Altimetry-driven Antarctic Circumpolar*
 607 *Current fronts*. SEANOE. Retrieved from <https://doi.org/10.17882/59800>
 608 doi: 10.17882/59800
- 609 Perlin, N., Kamenkovich, I., Gao, Y., & Kirtman, B. P. (2020, September). A
 610 study of mesoscale air–sea interaction in the Southern Ocean with a regional
 611 coupled model. *Ocean Modelling*, 153, 101660. Retrieved 2021-01-07, from
 612 <https://linkinghub.elsevier.com/retrieve/pii/S1463500320301621> doi:
 613 10.1016/j.ocemod.2020.101660
- 614 Rintoul, S. R. (2002). Ekman Transport Dominates Local Air–Sea Fluxes in Driving
 615 Variability of Subantarctic Mode Water. *Journal of Physical Oceanography*, 32,
 616 14.
- 617 Sallée, J.-B., Matear, R. J., Rintoul, S. R., & Lenton, A. (2012, August). Lo-
 618 calized subduction of anthropogenic carbon dioxide in the Southern Hemi-
 619 sphere oceans. *Nature Geoscience*, 5(8), 579–584. Retrieved 2021-11-08, from
 620 <http://www.nature.com/articles/ngeo1523> doi: 10.1038/ngeo1523
- 621 Sallée, J.-B., Wienders, N., Speer, K., & Morrow, R. (2006, December). Forma-
 622 tion of subantarctic mode water in the southeastern Indian Ocean. *Ocean Dynam-*
 623 *ics*, 56(5-6), 525–542. Retrieved 2021-01-07, from [http://link.springer.com/10](http://link.springer.com/10.1007/s10236-005-0054-x)
 624 [.1007/s10236-005-0054-x](http://link.springer.com/10.1007/s10236-005-0054-x) doi: 10.1007/s10236-005-0054-x
- 625 Sarmiento, J. L., Gruber, N., Brzezinski, M. A., & Dunne, J. P. (2004, Jan-
 626 uary). High-latitude controls of thermocline nutrients and low latitude bio-
 627 logical productivity. *Nature*, 427(6969), 56–60. Retrieved 2021-11-08, from
 628 <http://www.nature.com/articles/nature02127> doi: 10.1038/nature02127
- 629 Schneider, E. K., Kirtman, B. P., & Perlin, N. (2023). The role of atmospheric
 630 noise in decadal sst variability. *Journal of Climate*, 36(7), 2147 - 2166. Re-
 631 trieved from [https://journals.ametsoc.org/view/journals/clim/36/7/](https://journals.ametsoc.org/view/journals/clim/36/7/JCLI-D-22-0399.1.xml)
 632 [JCLI-D-22-0399.1.xml](https://journals.ametsoc.org/view/journals/clim/36/7/JCLI-D-22-0399.1.xml) doi: <https://doi.org/10.1175/JCLI-D-22-0399.1>
- 633 Seo, H., Miller, A. J., & Norris, J. R. (2016, February). Eddy–Wind Inter-
 634 action in the California Current System: Dynamics and Impacts. *Jour-*
 635 *nal of Physical Oceanography*, 46(2), 439–459. Retrieved 2020-06-08, from
 636 <http://journals.ametsoc.org/doi/10.1175/JPO-D-15-0086.1> doi:
 637 10.1175/JPO-D-15-0086.1
- 638 Sloyan, B. M., & Rintoul, S. R. (2001). Circulation, renewal, and modification of
 639 antarctic mode and intermediate water. *Journal of Physical Oceanography*, 31(4),
 640 1005 - 1030. Retrieved from [https://journals.ametsoc.org/view/journals/](https://journals.ametsoc.org/view/journals/phoc/31/4/1520-0485.2001.031.1005_cramoa.2.0.co.2.xml)
 641 [phoc/31/4/1520-0485.2001.031.1005_cramoa.2.0.co.2.xml](https://journals.ametsoc.org/view/journals/phoc/31/4/1520-0485.2001.031.1005_cramoa.2.0.co.2.xml) doi: 10.1175/1520-
 642 -0485(2001)031<1005:CRAMOA>2.0.CO;2
- 643 Small, R., deSzoeko, S., Xie, S., O'Neill, L., Seo, H., Song, Q., ... Minobe, S.
 644 (2008, August). Air–sea interaction over ocean fronts and eddies. *Dynam-*
 645 *ics of Atmospheres and Oceans*, 45(3-4), 274–319. Retrieved 2020-06-17, from

- 646 <https://linkinghub.elsevier.com/retrieve/pii/S0377026508000341> doi:
 647 10.1016/j.dynatmoce.2008.01.001
- 648 Smith, R., Jones, P., Briegleb, B., Bryan, F., Danabasoglu, G., Dennis, J., ... Yeager,
 649 S. (2010). The Parallel Ocean Program (POP) Reference Manual. *Community*
 650 *Climate System Model*, 141.
- 651 Speer, K., Rintoul, S. R., & Sloyan, B. (2000, December). The Diabatic Deacon
 652 Cell*. *Journal of Physical Oceanography*, 30(12), 3212–3222. Retrieved 2021-11-08, from [http://journals.ametsoc.org/doi/10.1175/1520-0485\(2000\)030<3212:TDDC>2.0.CO;2](http://journals.ametsoc.org/doi/10.1175/1520-0485(2000)030<3212:TDDC>2.0.CO;2) doi: 10.1175/1520-0485(2000)030<3212:TDDC>2.0.CO;2
- 653
 654
 655
- 656 Tozuka, T., & Cronin, M. F. (2014, April). Role of mixed layer depth in surface
 657 frontogenesis: The Agulhas Return Current front: Tozuka and Cronin: Frontogenesis:
 658 Role of mixed layer depth. *Geophysical Research Letters*, 41(7), 2447–2453.
 659 Retrieved 2020-06-05, from <http://doi.wiley.com/10.1002/2014GL059624> doi:
 660 10.1002/2014GL059624
- 661 Tozuka, T., Ohishi, S., & Cronin, M. F. (2018, July). A metric for surface heat flux
 662 effect on horizontal sea surface temperature gradients. *Climate Dynamics*, 51(1-
 663 2), 547–561. Retrieved 2020-06-05, from <http://link.springer.com/10.1007/s00382-017-3940-2> doi: 10.1007/s00382-017-3940-2
- 664
 665 Verdy, A., Dutkiewicz, S., Follows, M. J., Marshall, J., & Czaja, A. (2007,
 666 June). Carbon dioxide and oxygen fluxes in the Southern Ocean: Mechanisms of
 667 interannual variability: Southern Ocean Carbon and Oxygen Fluxes. *Global Biogeochemical Cycles*, 21(2), N/A–N/A. Retrieved 2021-10-24, from <http://doi.wiley.com/10.1029/2006GB002916> doi: 10.1029/2006GB002916
- 668
 669
 670 Wu, R., & Kirtman, B. P. (2005, August). Roles of Indian and Pacific Ocean
 671 air–sea coupling in tropical atmospheric variability. *Climate Dynamics*, 25(2-3),
 672 155–170. Retrieved 2021-10-18, from <http://link.springer.com/10.1007/s00382-005-0003-x> doi: 10.1007/s00382-005-0003-x
- 673
 674 Zhang, W., & Kirtman, B. (2019, March). Estimates of Decadal Climate Predictability
 675 From an Interactive Ensemble Model. *Geophysical Research Letters*, 46(6), 3387–3397.
 676 Retrieved 2021-10-18, from <https://onlinelibrary.wiley.com/doi/10.1029/2018GL081307> doi: 10.1029/2018GL081307
- 677

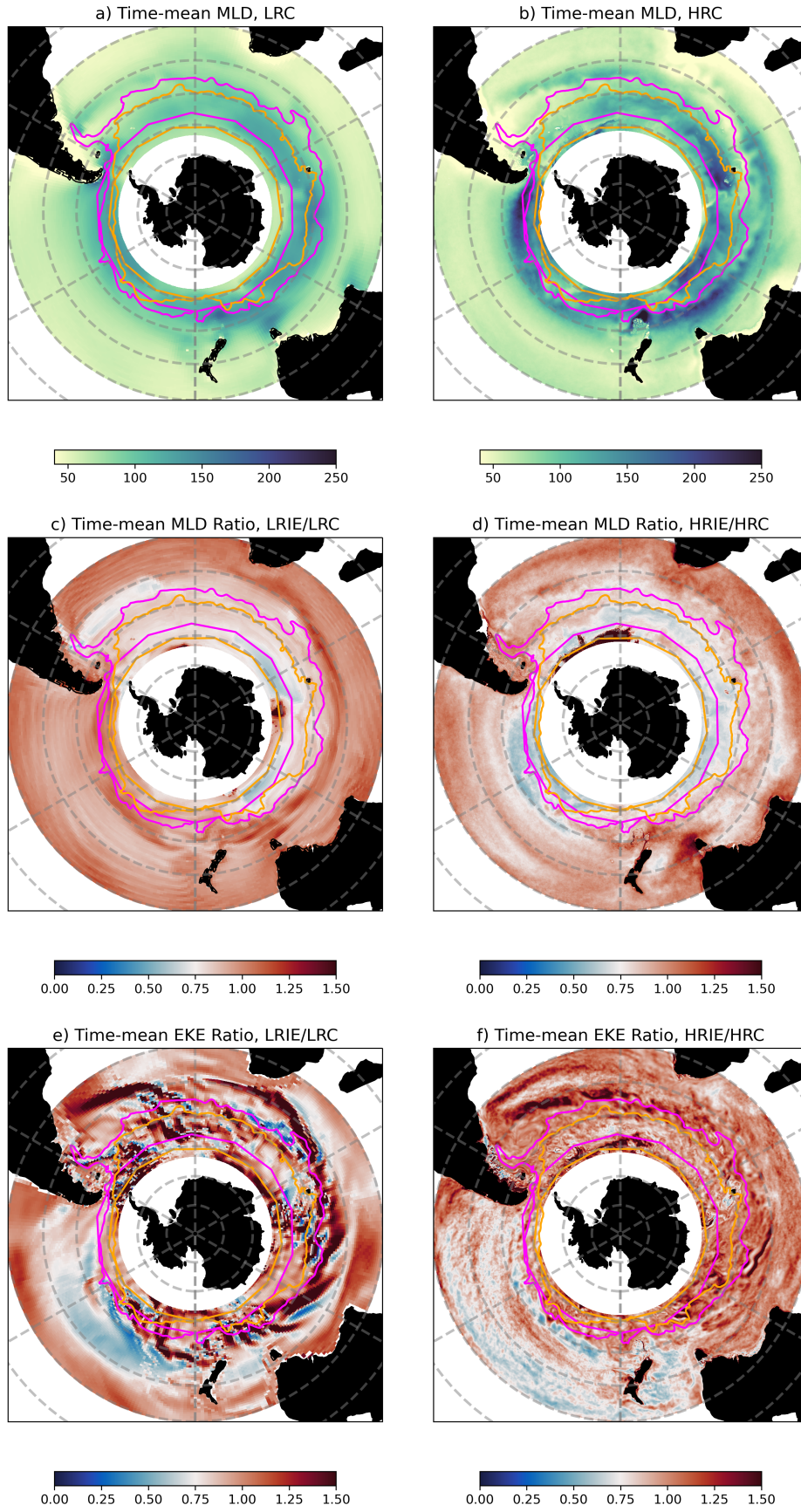


Figure 2. Time-mean MLD in a) LRC and b) HRC, from year 121 to 150. Polar Front (PF, orange line) and Subantarctic Front (SAF, magenta line).

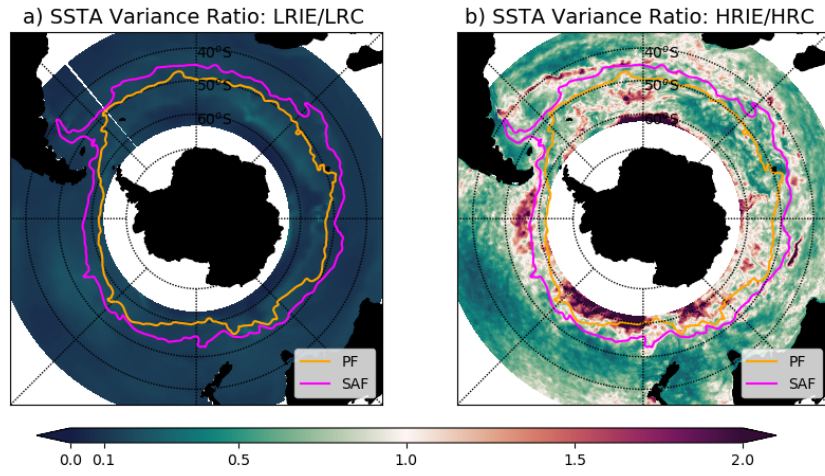


Figure 3. a) SSTA variance ratio of LRIE to LRC and b) SSTA variance ratio of HRIE to HRC. SSTA are the departures from the monthly SST climatology. Polar Front (PF, blue line) and Subantarctic Front (SAF, orange line).

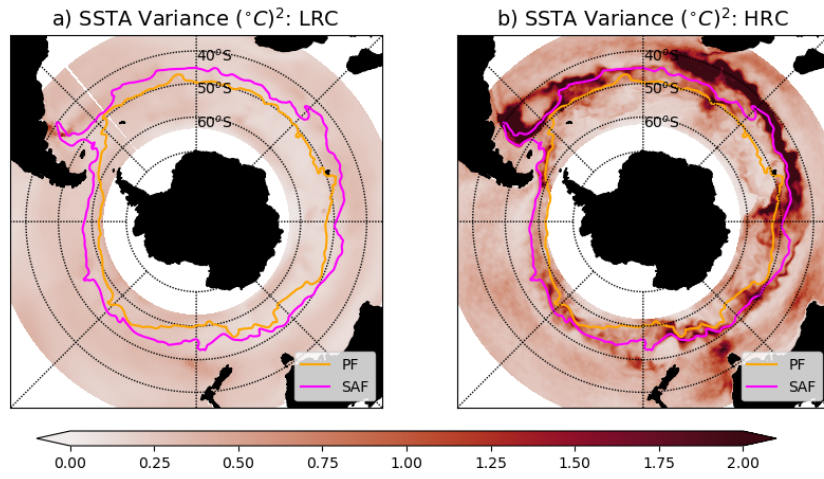


Figure 4. The variance of MLDA in a) LRC, b) HRC from year 121 to 150. SSTA anomalies (SSTAs) are defined as departures from the monthly climatology. Polar front (PF, orange line) and Subantarctic Front (SAF, magenta line).

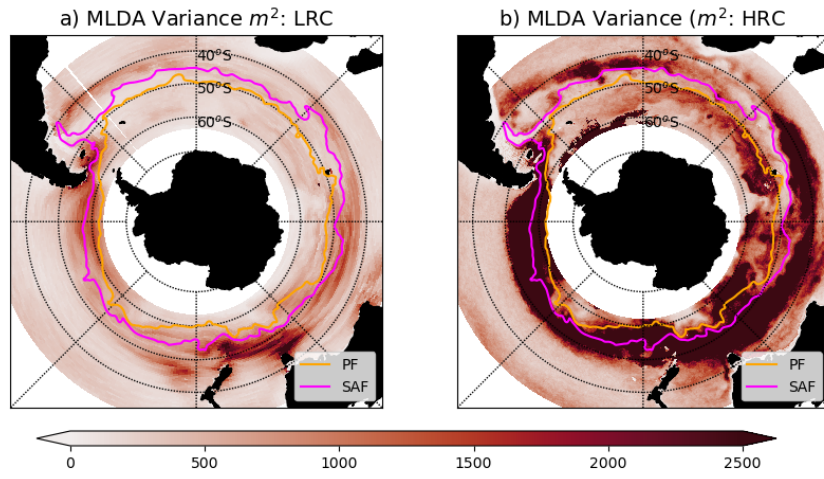


Figure 5. Variance of MLDA in a) LRC, b) HRC from year 121 to 150. MLD anomalies are defined as departures from the monthly climatology. Polar front (PF, orange line) and Subantarctic Front (SAF, magenta line).

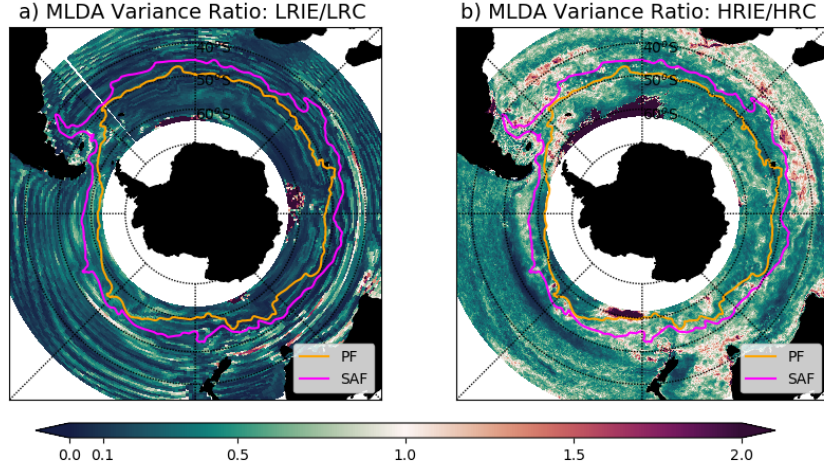


Figure 6. a) MLD variance ratio of LRIE to LRC and b) MLD variance ratio of HRIE to HRC. MLD anomalies are defined as departures from the monthly climatology. Polar Front (PF, blue line) and Subantarctic Front (SAF, orange line).

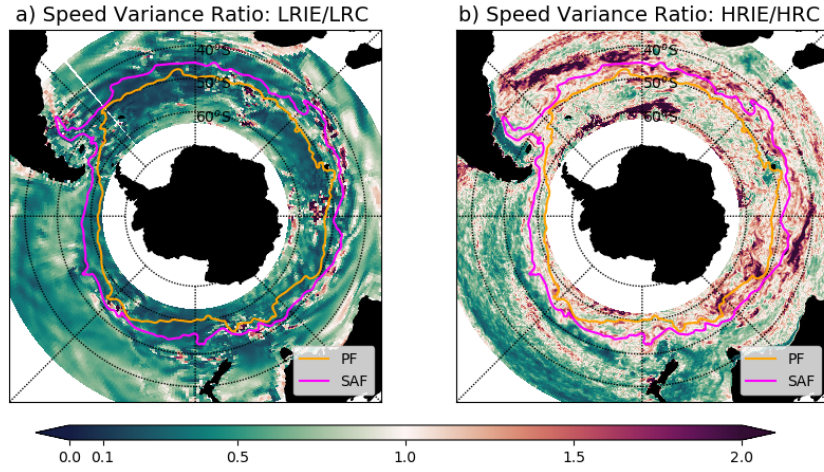


Figure 7. Surface current speed variance ratio in a) HRC and b) LRC, from year 121 to 150. Polar Front (PF, orange line) and Subantarctic Front (SAF, magenta line).

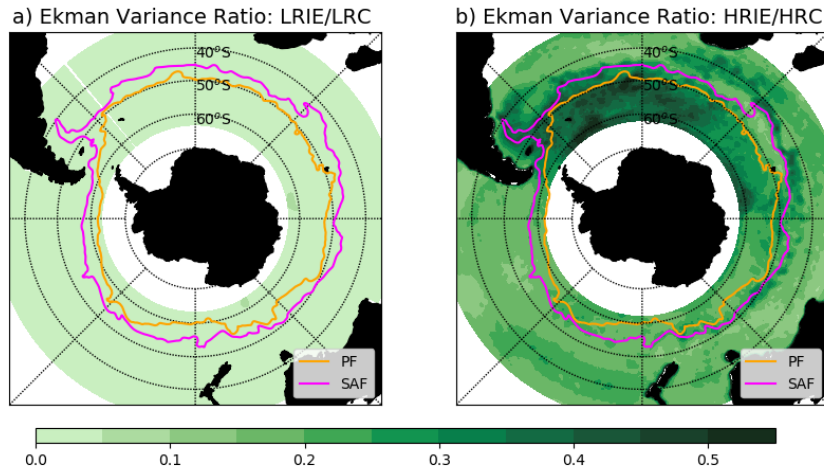


Figure 8. a) Ekman transport variance ratio of LRIE to LRC and b) Ekman transport variance ratio of HRIE to HRC. Polar Front (PF, blue line) and Subantarctic Front (SAF, orange line).